Dye-Sensitized Photoelectrochemical Cell Using a Nanocomposite SiO_2/Poly(Ethylene Glycol) Thin Film as Electrolyte Support. Characterization by Time-Resolved Luminescence and Conductivity Measurements

Elias Stathatos and Panagiotis Lianos*

Engineering Science Department, University of Patras, 26500 Patras, Greece

Christophoros Krontiras

Physics Department, University of Patras, 26500 Patras, Greece

Received: June 7, 2000; In Final Form: December 16, 2000

A dye-sensitized photoelectrochemical cell has been constructed by using a TiO_2 mesoporous film, a ruthenium bipyridyl derivative as photosensitizer, and a SiO_2/poly(ethylene glycol)-200 (SiO_2/PEG-200) nanocomposite thin film as electrolyte support. The TiO_2 film has been made by hydrolysis of titanium isopropoxide in Triton X-100 reverse micelles. In the present work, emphasis has been given to the nature and the applicability of the SiO_2/PEG-200 film, which has been characterized by conductivity and, mainly, time-resolved luminescence quenching techniques. It has been found that optimal cell function is obtained with a SiO_2/PEG-200 film where the PEG-200 content is about 10 wt %, a composition which is above and close to the percolation threshold for the PEG subphase.

Introduction

Dye sensitized photoelectrochemical cells (DSPEC) seem to be a low-cost alternative to conventional solid-state photovoltaic cells.[1] A lot of work has been recently devoted to their optimization, following the original discovery[2] that ruthenium bipyridyl derivatives adsorbed on nanostructured TiO_2 films and combined with liquid electrolytes can efficiently convert visible light to electricity.[2−6] Dye sensitization is the process where a dye adsorbed on a wide band gap semiconductor absorbs visible light and transfers the excited electron into the conduction band of the semiconductor. Even though, several wide band gap semiconductors have been studied in various dye-sensitization processes,[5,7,8] the most popular choice is TiO_2, a well-known, stable, nontoxic material which can be easily deposited as a nanostructured thin film. Attempts have also been made to fabricate DSPEC's with various sensitizers;[8−11] however, ruthenium bipyridyl derivatives[3] have proven themselves as the best choice to date. DSPEC's bearing a liquid electrolyte are more efficient systems than their equivalents, which employ a solid electrolyte material,[12] obviously, for charge mobility reasons. However, practical advantages and, possibly, greater stability of the cell may be gained when using a solid charge-transport system.[12−14] In the present work we concentrate our attention to this last question. We have fabricated a dye-sensitized photoelectrochemical cell where a I_3^-/I^- redox couple is supported in a nanocomposite thin film made of sol−gel silica and a poly(ethylene glycol) oligomer. Luminescence probing methods and conductivity measurements have been employed in order to characterize the nanocomposite material and find the optimum combination of organic/inorganic components for best ion transport and satisfactory DSPEC efficiency. I_3^-/I^- has been chosen as redox couple, since it is a standard choice[2,3,5,9,10] when combined with TiO_2 and Ru-bipyridyl photosensitizers.

* Corresponding author. Telephone: 30-61-997587. Fax: 30-61-997803. E-mail: lianos@upatras.gr.

Experimental Section

Materials. Titanium(IV) isopropoxide, tetramethoxysilane (TMOS), polyoxyethylene(10) isooctylphenyl ether (Triton X-100), poly(ethylene glycol)-200 (PEG-200), tris(2,2′-bipyridine)ruthenium dichloride hexahydrate ($Ru(bpy)_3^{2+}$), and methyl viologen (MV^{2+}) were purchased from Aldrich and used as received. *cis*-bis(isothiocyanato)bis(2,2′-bipyridyl-4,4′-dicarboxylato)ruthenium(II)[15] ($RuL_2(NCS)_2$) was provided by Solaronix SA (rue de l'Ouriette 129, 1170 Aubonne VD, Switzerland). The rest of the reagents were from Merck, while Millipore water was used in all experiments. Optically transparent electrodes (OTE) were cut from an indium−tin oxide (ITO) coated glass (<10 Ω/square) purchased from Pilkington-Flabeg, Germany.

Preparation of TiO2 Mesoporous Films Deposited on OTE-ITO Glasses. A reverse micellar solution of 0.2 M Triton X-100 and 0.4 M water was prepared in cyclohexane. To this solution we added 0.2 M titanium isopropoxide under vigorous stirring and at ambient conditions. Other concentrations of the above components have also been tried but optimal results were obtained with the present combination.[16] Hydrolysis and condensation of titanium isopropoxide begins as soon as it is introduced in the reverse micellar solution, but it takes about an hour before the solution becomes a visible gel.[16,17] The thus prepared composite material can be deposited as a thin film on an ITO slide by dip-coating. A 20 x 30 mm slide was cut from an ITO glass; it was sonicated for 20 min in ethanol and was, finally, copiously washed with Millipore water and dried in a stream of N_2. The thus prepared slide was dipped into the gelling solution at an early stage of gelation and was fast withdrawn at a speed of 2 cm/s. The composite organic−inorganic film was left to dry in air and the dipping was repeated 2 more times. The film was deposited on only the ITO side of the glass. The other side was covered with a tape. After the three dippings, the back tape was pealed off and the glass surface was locally

10.1021/jp0020642 CCC: $20.00
Published on Web 04/12/2001

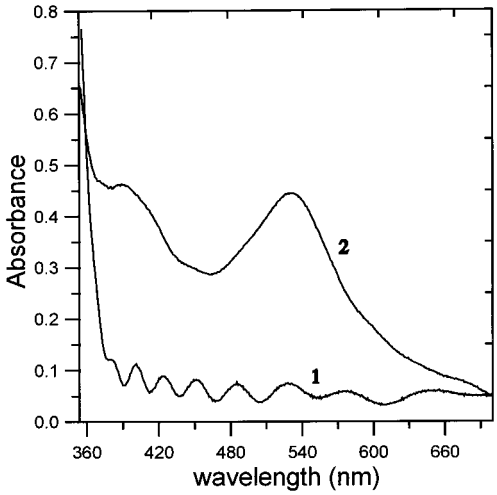

Figure 1. (1) Absorption spectrum of a standard TiO_2 film on a glass support. (2) Same film with adsorbed dye.

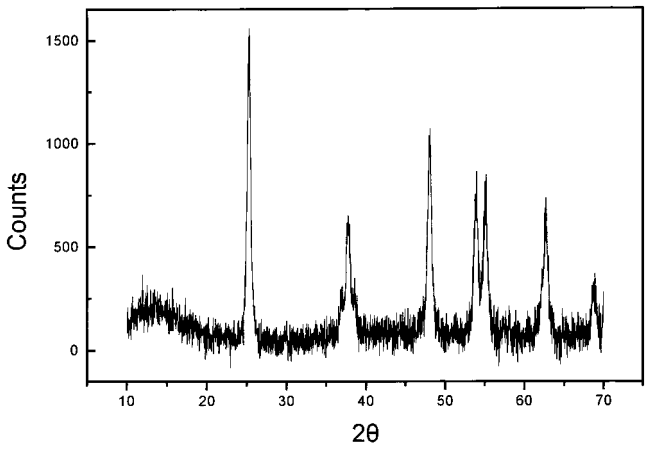

Figure 2. X-ray diffraction spectrum of titania powder obtained from titanium isopropoxide hydrolysis in reverse micelles followed by freeze-drying and calcination.

washed with acetone. Then the film was slowly heated in air, up to 450 °C, at a rate of 3.5 °C/min. The film was finally sintered at 450 °C for about 15 min more. The procedure was repeated two additional times so that 3 x 3 depositions were made. Its thickness was measured by profilometry and was found 1.2 μM. The obtained film was transparent. Thicker films could be made by further successive coatings; however, thickness grows at the expense of transparency. By using a thickness of 1.2 μM and by exploiting the interference fringes appearing in the absorption spectrum of the TiO_2 film, shown in Figure 1, a rough estimation was made for the film index of refraction, i.e., 1.74. This value is much lower than the tabulated index of refraction for crystalline titania. It is obviously due to the mesoporous structure of the film. Indeed, AFM and SEM images of the films prepared by the above method and published in previous publications[16−19] reveal a mesoporous structure that consists of TiO_2 nanoparticles of practically monodispersed size with exceptional reproducibility. The size of the nanoparticles can be easily controlled by choosing the water/surfactant ratio in the original reverse micellar solution.[18] Larger nanoparticles are made when more water exists in the solution. The advantage of the reverse-micellar route in making TiO_2 particles, as compared with other methods, exactly lies in this capacity to control the mesoporous structure of the obtained films. The diameter of the nanoparticles employed in the present work, as estimated by using AFM images, was around 30 nm.

Characterization of TiO2 Used in the Present Work by X-ray Diffraction. The TiO_2 films are too thin to give a detectable X-ray diffraction spectrum. We have freeze-dried the reverse micellar solution containing titanium isopropoxide about 1 h after mixing the components. The gel was first brought to liquid nitrogen temperature and then was continuously pumped, while the vessel containing the solution was exposed to ambient temperature. The solution remained frozen due to evaporation of the solvent and it remained so until all solvent had been evaporated. The obtained material contains, of course, TiO_2 and surfactant. It is then calcinated under the same conditions, as above-described for films. The obtained powder was studied by X-ray diffraction and it gave the spectrum of Figure 2, which corresponds to anatase. Given the conditions of the adopted procedure, we believe that the above film also consists of anatase nanocrystallites.

Procedure for the Adsorption of the Photosensitizer RuL2(NCS)2 on TiO2 Films. When the TiO_2 film was taken out of the furnace and while it was still hot, it was dipped into a 1 mM ethanolic solution of $RuL_2(NCS)_2$ and was left there for about 24 h. Then it was copiously washed with ethanol, dried in a stream of N_2, and studied by absorption spectrophotometry. The dye was steadily attached on the TiO_2 film, obviously, by means of its carboxylate groups.[15,20] Figure 1 shows the absorption spectra of the TiO_2 film with and without the adsorbed dye. The absorption of visible light by the film is, obviously, possible only through the dye.

Formation of the Composite SiO2/PEG-200 Film Containing Electrolyte. On the top of the TiO_2/dye layer, a thin composite organic/inorganic film containing I_3^-/I^- has been deposited under the following procedure, which was carried out at ambient conditions. TMOS was partially hydrolyzed by mixing with acidified water (HCl, pH 3.0) at a molar ratio TMOS:water = 1:2. The mixture was stirred for 1 h. It was originally turbid but it became clear in the course of proceeding hydrolysis. Then to 1 mL of this sol, we added 5 g of an aqueous PEG-200 solution containing the redox couple. In particular, I_2 was diluted in pure PEG-200, while KI was diluted in water. Then the two solvents were mixed and produced a transparent solution. Only if I_2 is first diluted in PEG-200, it can finally produce a transparent solution, since it is not directly soluble in water. Different PEG-200/water ratios have been obtained for the purpose of the present work, while the overall concentration was 0.03 M for I_2 and 0.3 M for KI. After mixing with prehydrolyzed TMOS, the solution was stirred for 4 h, when it was judged ready for application. During that time a condensation procedure goes on by −Si−O−Si− polymerization, slowly producing a gel. 4 h of waiting time under stirring still leaves the solution at an early stage of gelation. A thin film of this composite material was deposited by dip-coating. As before, the back inactive side of the glass support was covered with a tape before dipping and was pealed off afterward.

Application of the Counter Electrode That Ends the Fabrication of the Cell. On the top of the SiO_2/PEG-200/electrolyte layer, an ITO electrode covered with a thin Pt film was placed and pressed against the underlying support. Si−O-bridges help binding the counter electrode so that the composite SiO_2/PEG-200 material additionally acts in holding the parts of the cell together in a stable thin sandwich configuration. Pt was applied prior to cell binding by vacuum evaporation on the ITO slide. Its presence is necessary to improve cell performance.

SiO2/PEG-200 Films Prepared for Conductivity Measurements. Conductivity measurements were made with thin films of the nanocomposite material containing 0.03M I_2 and 0.3 M

KI in the absence of titania, dye, or Pt, i.e., the rest of the components of the cell. In the case of impedance measurements, the material was sandwiched between two plain ITO slides. In the case of steady-state conductivity measurements, thin films of SiO_2/PEG-200 were deposited on plain glass by dip-coating. Four contacts were made with silver paint at the four corners of a square-centimeter sample.

SiO2/PEG-200 Films Used for Time-Resolved Luminescence Probing Studies. The films used for luminescence probing were deposited on plain glass and did not contain I_2 or KI but they were enriched with $Ru(bpy)_3^{2+}$ and MV^{2+}. Both substances were solubilized in the water used to make the PEG-200/water mixtures. The overall concentration of $Ru(bpy)_3^{2+}$ in solution was always 1 mM, while the concentration of MV^{2+} varied from 5 to 20 mM. Such concentrations are necessary in order to transfer a sufficient quantity of probe and quencher in the film and obtain detectable signals. Repeated experiments, based on absorption spectrophotometry, showed that the amount of probe and quencher transferred into the film is proportional with the concentration in solution. Prior to measurements, films were heated above 70 °C to ensure evaporation of volatile components.

Methods. Absorption measurements were made with a Cary 1E spectrophotometer. Dielectric relaxation measurements were performed with a Solartron 1260 impedance gain-phase analyzer equipped with a Novocontrol BDC converter. The temperature control was achieved by placing the samples on an INSTEC STC400 hot stage. Steady-state conductivity measurements were made by the Van der Pauw technique (four-point method). X-ray diffraction measurements were made with a Philips PW 1840 diffractometer. Incident photon to current efficiency (IPCE%) values[1] have been measured by illumination of the samples with a 250-W Phillips tungsten halogen lamp through a filter monochromator (Oriel-7155). The lamp spectrum satisfactorily simulates solar radiation at the surface of the earth. The number of incident photons was calculated by employing a radiant power/energy meter (Oriel-70260). Time-Resolved luminescence decay profiles were recorded with the single-photon-counting technique using a homemade nanosecond hydrogen flash lamp and ORTEC electronics. The installation has been tested by recording decay profiles of the present ($Ru(bpy)_3^{2+}$) and other luminophores in different environments and comparing our results with those found in the literature. Temperature control was obtained by placing the samples in a holder thermostated by circulating water.

Analysis of the Luminescence Decay Profiles. To judge the capacity of the composite SiO_2/PEG-200 material to allow diffusion of charged mobile species within it, we have studied the diffusion-controlled quenching kinetics of a cationic luminophore by a cationic quencher. These species are expected to be solubilized in the organic subphase by complexation with the PEG chains. The luminescence decay profiles of $Ru(bpy)_3^{2+}$ in the presence of MV^{2+} were analyzed by a model of stretched exponentials given by the following equation:[21−24]

$$I(t) = I_0 \exp(-t/\tau_o) \exp[-C_1(t/\tau_o)^f + C_2(t/\tau_o)^{2f}] \qquad 0 < f < 1 \tag{1}$$

while the first-order quenching rate constant was calculated by

$$K(t) = (1/\tau_o)[fC_1(t/\tau_o)^{f-1} - 2fC_2(t/\tau_o)^{2f-1}] \tag{2}$$

C_1, C_2, and f are parameters calculated by fitting eq 1 to the experimental decay profile and used to calculate the values of $K(t)$. τ_o is the decay time in the absence of quencher and it is measured in separate experiments. The distribution of the residuals and the autocorrelation function of the residuals was used as fitting criterion. Experience has shown that combination of these two criteria offers parameter values with high precision (error less than 5%) and repeatability. More information about this model and of its application in the study of nanocomposite materials is given in ref 24.

The model of eq 1 applies to any quenching reaction where an excited luminophore can, in principle, be quenched by any quencher present. Thus it applies to electron or energy-transfer as well as to diffusion-controlled quenching. It is particularly fit to complex systems with unknown but, certainly, restricted geometry. It is also particularly fit to the present system where information on molecular diffusion is obtained by analysis of the luminescence decay profiles. The model is based on the fundamental kinetics of restricted reactions where a reactant behaves as a random walker. In a restricted environment, the number of distinct sites visited by the random walker within a time interval, t, is not proportional to t but to t^f, where $0 < f < 1$, hence the noninteger power of time in eq 1. Obviously, the restrictions imposed by the reaction domain reflect on the value of f, f being smaller in more restricted reactions. In the development of the decay law for quenching in restricted geometries,[25] it is found that the second exponential of eq 1 should, actually, contain an infinite number of terms. The first two terms in the series have a specific meaning.[21,25] The first is proportional to the number of distinct sites visited within a time interval and the second to its variance. In theoretically produced luminescence decay profiles or for data recorded without noise, fitting with eq 1 is impossible.[23] When the decay profile is recorded with a large number of data, with Gaussian distribution, as with the single photon-counting technique presently used, only the number of distinct sites visited and its variance are quantities different from zero.[21] For this reason, the two terms of the second exponential in eq 1 suffice to fit the experimental decay profile. This approximation gives very satisfactory results.

The rate constant is time-dependent in all cases where the model of eq 1 applies, since it then depends on the distance between the reacting species. Distance dependence creates time dependence, which becomes even more intense in the case of restricted geometries. Thus the value of K in eq 2 is time-dependent. Since it is difficult to tabulate any $K(t)$-value for any value of time, we usually choose to tabulate only its value K_1 at the first time channel and its value K_L at the last recorded time channel. Then K_1 represents the rate constant at short times and K_L the rate constant at long times. Both K_1 and K_L are, of course, first-order rate constants and thus they depend on quencher concentration.

Variants of the above model of stretched exponentials have been systematically used in the past by various authors to study, in particular, interactions in solid-state materials. The donor decay model for resonance energy transfer quenching is the best known model of stretched exponentials.[26] The exponent f in that model is 0.5, when the reaction occurs between homogeneously and isotropically distributed donors and acceptors. Blumen et al. have then showed that in restricted environments f depends on the dimensionality of the reaction configuration.[25,27] Argyrakis and Kopelman have demonstrated the scaling laws that apply to diffusion in percolating clusters.[28,29] The presently used model, based on these previous studies, takes advantage of time-resolved analysis to follow molecular diffusion and interaction in complex systems with nonspecific geometry.

TABLE 1: Data Obtained by the Analysis of the Luminescence Decay Profile of $Ru(bpy)_3^{2+}$ in the Presence of Varying MV^{2+} Concentration in a Composite Silica/PEG-200 Film That Corresponds to a PEG-200 Content in the Original Sol Equal to 4 wt %[a]

quencher concn, mM	f	K_1, 10^6 s^{-1}	K_L, 10^6 s^{-1}	$10^2(K_L/K_1)$
5	0.41	5.5	0.2	3.6
10	0.42	10	0.4	4.0
13	0.42	53	0.8	1.5
16	0.41	59	1.0	1.7
20	0.42	65	1.1	1.7

[a] The concentration of $Ru(bpy)_3^{2+}$ in the sol was 1 mM. The concentrations of MV^{2+} shown are also measured in the original sol. The decay time of $Ru(bpy)_3^{2+}$ in the absence of quenching was 845 ns. The measurements were made at 20 °C.

TABLE 2: Data Obtained by the Analysis of the Luminescence Decay Profile of $Ru(bpy)_3^{2+}$ in the Presence of Varying MV^{2+} Concentration in a Composite Silica/PEG-200 Film That Corresponds to a PEG-200 Content in the Original Sol Equal to 14 wt %[a]

quencher concn, mM	f	K_1, 10^6 s^{-1}	K_L, 10^6 s-1	$10^2(K_L/K_1)$
5	0.83	0.8	0.5	63
10	0.84	1.3	0.8	62
13	0.82	2.2	1.1	50
16	0.84	4.4	1.5	34
20	0.83	4.7	1.8	38

[a] The concentration of $Ru(bpy)_3^{2+}$ in the sol was 1 mM. The concentrations of MV^{2+} shown are also measured in the original sol. The decay time of $Ru(bpy)_3^{2+}$ in the absence of quenching was 1050 ns. The measurements were made at 20 °C.

Results and Discussion

Organic/inorganic nanocomposite gels comprising poly(ethylene glycol) oligomers and silica particles synthesized through a sol−gel method are biphasic systems in which silica aggregates are wrapped around the polymer phase.[30] The disordered nature of these materials, the small size of the individual domains, and the strong differences between their dynamic behavior preclude the application of microscopy and necessitates the employment of several spectroscopic techniques for their characterization.[31] The composition of the original sol, which dictates the final composition of the film, determines the mechanical properties of the final material. More stable films are made with a smaller percentage of PEG, i.e., a larger percentage of silica. However, too small a percentage of the organic phase limits ion transport mobility. One way to think of the quality and the efficiency of the nanocomposite material, within the scope of the present work, is to search for the formation of a percolating cluster by the organic subphase within the inorganic embedding phase. A percolating cluster, close to the percolation threshold, provides favorable conditions for satisfying both good mechanical properties, since it corresponds to maximum silica content, and good ion transport properties, since it corresponds to just enough of the organic phase to allow the existence of interconnecting ion transport channels. In our opinion, the best way to study a percolation cluster is to use time-resolved luminescence quenching techniques, as in the following paragraph.

Luminescence Probe Characterization of Nanocomposite SiO2/PEG-200 Films. In the data presented in this paragraph, we have registered and analyzed the luminescence decay profiles of $Ru(bpy)_3^{2+}$ in the presence of varying MV^{2+} concentrations in different nanocomposite films made at different PEG-200/water mass ratios. PEG-200 is an oligomer (4−5 ethylene oxide units) where the number 200 corresponds to its approximate molecular weight. Both luminophore and quencher probe the organic phase,[32] since, being dicationic, they form strong complexes with PEG, through ether oxygen.

Tables 1 and 2 show data of the analysis of luminescence decay profiles by means of eqs 1 and 2. These experimental results correspond to 20 °C measurements. Henceforth, the concentration of PEG is shown as weight fraction (%) over the total weight of the sol, including silica. The PEG concentration, as well as that of the luminescence probe and its quencher, increases when transferred to the film, because of solvent evaporation. However, we believe that the relative molar ratios of silica, PEG, and the incorporated inorganic and organic ionic species remain the same in solution and in the corresponding film. Table 1 corresponds to a film made from a sol where PEG-200 content was 4 wt %. As will be shortly shown, this is a case below the percolation threshold of the organic subphase. Table 2 presents data for a characteristic case above percolation threshold, corresponding to a PEG-200 % age equal to 14 wt %. In the first case f values are around 0.42, while in the second case f values are larger than 0.8. In fact the variation of the value of f with respect to the organic content in the nanocomposite material is given in Figure 3. The f curve presents a smooth breaking point around 8% PEG. It increased fast below 8% PEG, but it increased at a much slower rate above this critical point. The value of f was 0.67 (i.e., $^2/_3$) in the concentration domain between 6 and 7 wt % PEG-200, for measurements at 20 °C. $f = 0.67$ corresponds to the value at the percolation threshold.[33,34] We have thus detected the critical concentration domain in which a percolation cluster is formed at 20 °C under the present conditions. This percolation cluster consists of the organic subphase and it explains the behavior of the f curve. Indeed, since both luminescence probes are associated with the organic subphase and they can diffuse exclusively within that phase, a percolation behavior for luminescence quenching is detected as soon as a percolation cluster is formed. Optimal conditions for DSPEC function are then defined just above the percolation threshold in the sense that PEG content should be large enough to ensure sufficient charge-carrier mobility but at the same time small enough to ensure good mechanical properties for the obtained film.

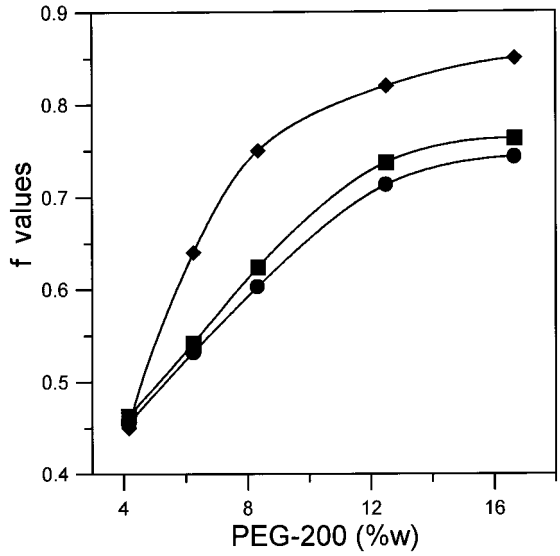

Figure 3. f-values vs PEG-200 wt % at various temperatures: (♦) 20 °C; (■) 45 °C; (●) 65 °C. The PEG-200 content was measured in the original sol.

The rest of the data in Tables 1 and 2 are in line with the existence or not of percolation in the organic subphase. Column 3 shows K_1 values. The rate constant at short times (see end of the Experimental section) suffers a large decrease above percolation threshold. The reason is that the reacting species are quasi-localized in limited areas at low organic content when the system is below percolation. Localization of the reacting species increases the effective quencher concentration and subsequently increases the probability of immediate reaction. Above percolation threshold the reacting species are dispersed and this results in smaller early-time reaction probabilities. As expected, K_L, the long-time rate constant, changes in inversely; i.e., it increases above the percolation threshold (column 4). The importance of the short-time vs long-time quenching probability is eloquently demonstrated by the values of the K_L/K_1 ratio below and above the percolation threshold (column 5). As expected, the luminescence quenching reaction mainly occurs at short times below threshold, but it is distributed over longer times above threshold and this is demonstrated by the dramatic increase of K_L/K_1 above threshold.

The behavior of the system at elevated temperatures is also seen in Figure 3. The data of this figure demonstrate a rather unexpected behavior. Thus the maximum f value was smaller at higher temperature, indicating a more restricted environment. Most physical systems facilitate molecular motion at elevated temperatures. The fact that the present system acts in the opposite direction indicates that the nanocomposite material undergoes a structural evolution at elevated temperature that makes percolation conditions stricter than at 20 °C. This is also seen by the fact that the value of $f = 0.67$, i.e., the percolation threshold, is then attained at higher polymer content, i.e., approximately 10%. As already said, the films are preheated above 70 °C before measurements. So we preclude the possibility that water entrapped in the films that goes out at elevated temperatures might be responsible for the above effect. It is highly probable that the PEG phase transition with temperature might be at the origin of the behavior of f. This question is further studied in our laboratories. It is anyhow advisable to work with a PEG content $\geq$10 wt % in order to obtain a cell that works sufficiently well at all ambient conditions.

Characterization of Composite SiO2/PEG-200 Films by Conductivity Measurements. Luminescence quenching probes relatively short-range ion displacement. We have proceeded by studying the nanocomposite ionic conductor with conductivity measurements, both by steady-state and dielectric relaxation, which probe the material on a larger area and on a longer-range ion displacement. We have first examined SiO_2/PEG-200 films deposited on plain glass, in the low PEG content domain, by steady-state four point conductivity measurements. The results are shown in Figure 4a. No measurements have been made above 16 wt % PEG, since the quality of the film was poor at such relatively high organic content. It is noted that conductivity increases, as expected, with PEG content. The increase, is, however, not linear, but it seems to be accelerated above 8 wt % PEG. In view of the data of the previous paragraph, it is obvious that the conductivity of the nanocomposite gel electrolyte is important when the system is above percolation threshold. To have a more representative configuration of the cell structure, we have also examined SiO_2/PEG-200 films sandwiched between ITO glass electrodes, in the low PEG content domain, by dielectric relaxation (impedance) measurements with respect to PEG content variation. The results are shown in Figure 4a,b. In all studied cases, it was found that the specific conductivity increased with the frequency of the applied

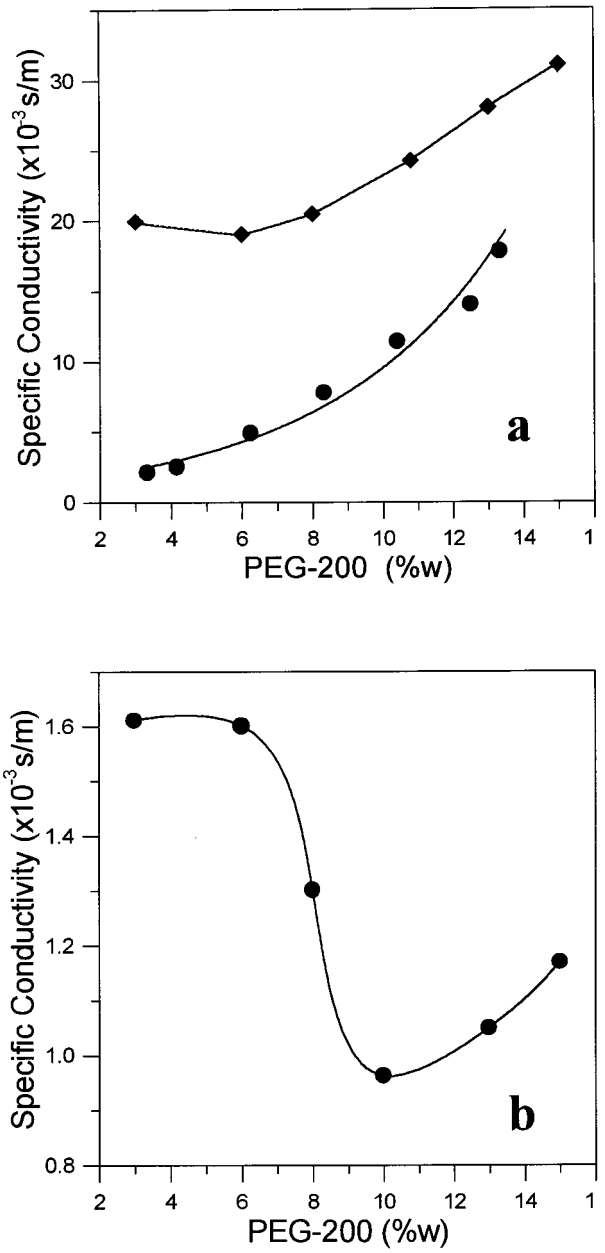

Figure 4. Specific conductivity vs PEG weight percent: (a) (●) steady-state measurements; (♦) impedance measurements at 7000 Hz; (b) impedance measurements at 100 Hz. The PEG-200 content was measured in the original sol. T = 25 °C.

voltage, achieving a plateau above 10^3 Hz. This is typical behavior for a fast ionic conductor. Figure 4a shows the evolution of specific conductivity with respect to PEG content, in the range 2−16%. The curve is drawn for a high frequency (7000 Hz), where the system gives high conductivity. The specific conductivity-versus-composition curve was similar to the steady-state curve. Conductivity increased with PEG content but increased faster above percolation, underlying the importance of percolation phenomena in the behavior of the ionic conductor. It is, however, interesting to observe the system behavior in the low-frequency (100 Hz) and low-conductivity range. Figure 4b shows that when the system enters the percolation domain, an abrupt change in specific conductivity is observed with a minimum at about 9 wt % PEG. Obviously the system undergoes a structural change in passing across the percolation threshold. It is then obvious that both luminescence quenching and conductivity measurements detect a percolation transition

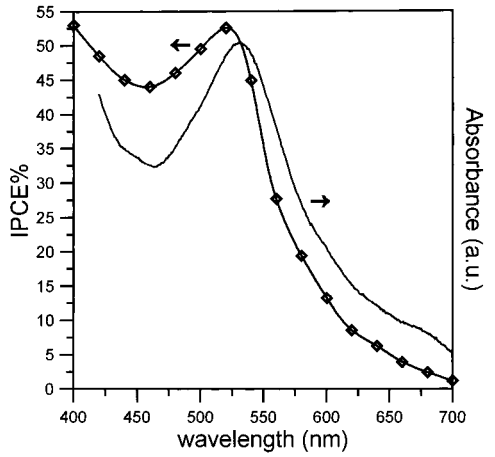

Figure 5. IPCE% values and adsorbed-dye absorbance vs illumination wavelength. T= 25 °C. PEG-200 content was 10 wt %.

that affects the ion-transporting properties of the present ionic conductor. The effect of temperature on conductivity was examined only above the percolation threshold. Conductivity then demonstrated a "normal" behavior; i.e., it increased with temperature. In comparison with the luminescence probing data and in view of the unexpected behavior of the *f* values with respect to temperature, we could conclude that conductivity data support the fact that water contained in the films is not responsible for the behavior of *f*. Otherwise it would similarly affect also conductivity data. It is also concluded that a mesoscopic structural transformation, obviously, related to the PEG subphase, should be responsible for the behavior of *f* not affecting a long-range transport phenomenon such as conductivity.

With these data in mind, we have proceeded with the construction and the testing of cells at various SiO_2/PEG-200 film compositions both above and below percolation threshold.

Efficiency of the Proposed DSPEC. Our above approach for fabricating the electrolyte support was rewarded by the obtained efficiencies of the present DSPECs. We have constructed cells by employing SiO_2/PEG-200 films made at various PEG-200 wt %. The efficiency of each cell is expressed in terms of the maximum IPCE value, which is located very close to the wavelength corresponding to the maximum of absorption of the dye sensitizer. Indeed, as seen in Figure 5, presenting IPCE values at different illumination wavelengths together with dye absorption spectrum, the maximum of cell efficiency practically coincides with the maximum of dye absorption. This is a sound demonstration of the dye-sensitization process, and it dictates the choice of illumination wavelength for maximum efficiency. It should be noted at this point that the measured IPCE values are in fact lower limits, and the actual values should be larger if the real number of absorbed photons were known. As seen in Figure 1, the optical density of the photosensitizer is around 0.4, which means that only 60% of the incident photons are absorbed. In fact, light is further absorbed by reflection on the counter electrode. Since IPCE is calculated under the assumption that all incident photons are absorbed by the dye, the recorded IPCE values are obviously underestimated. The values of maximum IPCEs for six different cells are shown in Figure 6. It is seen that the cell efficiency rapidly increases when the PEG content passes through the percolation threshold, achieving values above 50%. The efficiency continues to increase at a much slower rate above percolation threshold; however, when PEG content is $\geq$16%, the nanocomposite gel is no longer a solid and it is incapable of holding the cell parts

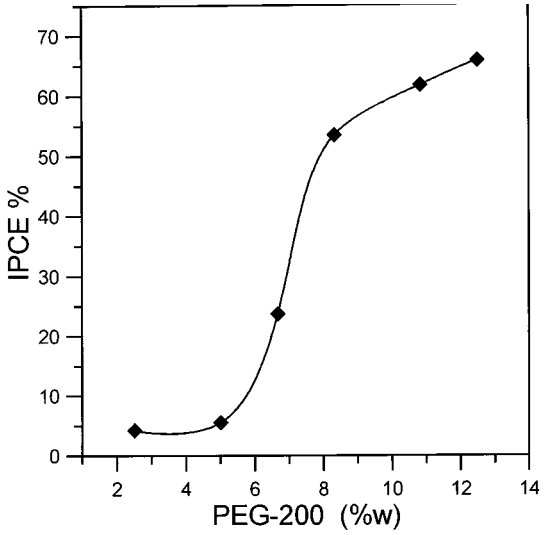

Figure 6. Maximum cell efficiency values (IPCE%) vs PEG-200 wt %. The PEG-200 content was measured in the original sol. T = 25 °C.

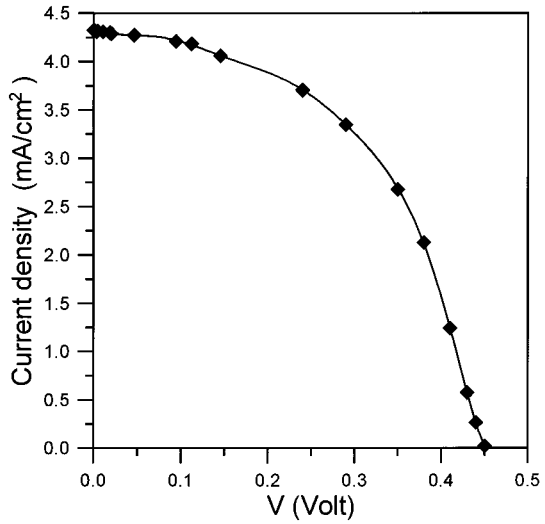

Figure 7. *I*−*V* curve for a cell made with 10 wt % PEG. Illumination was made by white light of 96 mW/cm^2 (about AM1.5 solar). T = 25 °C.

together any longer. For this reason, a typical cell was constructed with 10 wt % PEG. Its performance is seen in the *I*−*V* curve of Figure 7. By illumination with diffuse light of 96 mW/cm^2 (about AM 1.5 solar) the open circuit voltage was 0.47 V and the short circuit current was 4.3 mA/cm^2.

An important question that can be asked on these cells is about the role of the adsorbed water in their performance. Water comes in large fractions in the precursor sols. Upon film formation, part of it is evaporated but an important part is expected to be adsorbed in the pores of the titania film and in the nanocomposite gel. Its presence is expected to play a role in the cell performance, albeit small. We believe that given the satisfactory performance of the cell, further studies could provide conditions for cell-performance optimization. Another question is about the stability of the cell performance. The cell was found 97% stable after a 24-h illumination. We believe that there is ground for improving stability by proper sealing and moisture elimination.

Conclusion

A dye sensitized photoelectrochemical cell has been constructed in a sandwich configuration by layer deposition of

composite organic/inorganic materials. The present work has paid special attention to the properties of a nanocomposite SiO_2/PEG-200 layer used as electrolyte support. It has been demonstrated that a nanocomposite film embedding enough organic (PEG-200) material to provide percolation conditions just above the percolation threshold also offers very good conditions for photovoltaic conversion efficiency. The maximum IPCE(%) value obtained was $\geq 50\%$, which is considered satisfactory for a device employing a solid ionic conductor.

Acknowledgment. We are grateful to Prof. P. Koutsoukos for the X-ray diffraction measurements. We acknowledge financial aid from the program "K ΚΑΡΑΘΕΟΔΩΡΗΣ" of the University of Patras.

References and Notes

(1) Bach, V.; Lupo, D.; Comte, P.; Moser, J. E.; Weissoertel, F.; Salbeck, J.; Spreitzer, H.; Graetzel, M. *Nature* **1998**, *395*, 583.
(2) O'Reagan, B.; Graetzel, M. *Nature* **1991**, *353*, 737.
(3) Nazeeruddin, M. K.; Kay, A.; Rodicio, I.; Humphry-Baker, R.; Mueller, E.; Liska, P.; Vlachopoulos, N.; Graetzel, M. *J. Am. Chem. Soc.* **1993**, *115*, 6382.
(4) Huang, S. Y.; Schlichthoerl, G.; Nozik, A. J.; Graetzel, M.; Frank, A. J. *J. Phys. Chem.* **1997**, *101*, 2576.
(5) Bedja, I.; Kamat, P. V.; Hua, X.; Lappin, A. G.; Hotchandani, S. *Langmuir* **1997**, *13*, 2398.
(6) Bechinger, C.; Ferrere, S.; Zaban, A.; Sprague, J.; Gregg, B. A. *Nature* **1996**, *383*, 608.
(7) Sayama, K.; Sugithara, H.; Arakawa, H. *Chem. Mater.* **1998**, *10*, 3825.
(8) Liu, D.; Kamat, P. V. *J. Electrochem. Soc.* **1995**, *142*, 835.
(9) Vogel, R.; Hoyer, K.; Weller, H. *J. Phys. Chem.* **1994**, *98*, 3183.
(10) Deb, S. K.; Ellingson, R.; Ferrere, S.; Frank, A. J.; Gregg, B. A.; Nozik, A. J.; Park, N.; Schlichthoerl, G. *Paper presented in the 2nd world conference and excibition on photovoltaic solar energy conversion;* Vienna, Austria, 1996.
(11) O'Reagan, B.; Schwartz, D. T. *J. Appl. Phys.* **1996**, *80*, 4749.
(12) Matsumoto, M.; Miyazaki, H.; Matsuhiro, K.; Kumashiro, Y.; Takaoka, Y. *Solid State Ionics* **1996**, *89*, 263.
(13) Cao, F.; Oskam, G.; Searson, P. C. *J. Phys. Chem.* **1995**, *99*, 17071.
(14) O'Reagan, B.; Schwartz, D. T. *Chem. Mater.* **1998**, *10*, 1501.
(15) Liska, P.; Vlachopoulos, N.; Nazeeruddin, M. K.; Comte, P.; Graetzel, M. *J. Am. Chem. Soc.* **1988**, *110*, 3686.
(16) Stathatos, E.; Lianos, P.; DelMonte, F.; Levy, D.; Tsiourvas, D. *Langmuir* **1997**, *13*, 4295.
(17) Stathatos, E.; Lianos, P.; DelMonte, F.; Levy, D.; Tsiourvas, D. *J. Sol-Gel Sci. Technol.* **1997**, *10*, 83−89.
(18) Stathatos, E.; Tsiourvas, D.; Lianos, P. *Colloids Surf., A* **1999**, *149*, 49−56.
(19) Stathatos, E.; Lianos, P.; Couris, S. *Appl. Phys. Lett.* **1999**, *75*, 319.
(20) Heimer, A. T., Bignozzi, A. C., Meyer, J. G. *J. Phys. Chem.* **1993**, *97*, 11 987−11 994.
(21) Lianos, P. *Heterogeneous Chem. Rev.* **1996**, *3*, 53.
(22) Bekiari, V.; Lianos, P. *J. Colloid Interface Sci.* **1996**, *183*, 552.
(23) Lianos, P.; Argyrakis, P. *J. Phys. Chem.* **1994**, *98*, 7278.
(24) Bekiari, V.; Ferrer, M.-L.; Lianos, P. *J. Phys. Chem. B* **1999**, *103*, 9085.
(25) Klafter, J.; Blumen, A. *J. Chem Phys.* **1984**, *80*, 875.
(26) Lakowicz, J. R. *Principles of Fluorescence Spectroscopy*; Plenum Press: New York, **1983**.
(27) Klafter, J.; Blumen, A.; Zumofen, G. *J. Lumin.* **1984**, *31, 32*, 627.
(28) Argyrakis, P.; Kopelman, R. *J. Chem. Phys.* **1986**, *84*, 1047.
(29) Lindenberg, K.; Sheu, W.-S.; Kopelman, R. *J. Stat. Phys.* **1991**, *65*, 1269.
(30) Lesot, P.; Chapuis, S.; Bayle, J. P.; Rault, J.; Campero, A.; Judeinstein, P. *J. Mater. Chem.* **1998**, *8*, 147 and references therein.
(31) Brik, M. E.; Titman, J. J.; Bayle, J. P.; Judeinstein, P. *J. Polym. Sci., Part B: Polym. Phys.* **1996**, *34*, 2533 and references therein.
(32) Bekiari, V.; Ferrer, M.; Stathatos, E.; Lianos, P. *J. Sol−Gel Sci. Technol.* **1998**, *13*, 95.
(33) Rammal, R.; Toulouse, G. *J. Phys. Lett.* **1983**, *44*, L13.
(34) Alexander, S.; Orbach, R. *J. Phys. Lett.* **1982**, *43*, L625.